Research Article

The Ultimate Ballistic Drift Velocity in Carbon Nanotubes

Mohammad Taghi Ahmadi,[1] Razali Ismail,[1] Michael L. P. Tan,[1, 2] and Vijay K. Arora[1, 3]

[1] *Department of Electronic Engineering, Faculty of Electrical Engineering, Universiti Teknology Malaysia, 81310 Skudai, Johor Darul Takzim, Malaysia*

[2] *Electrical Engineering Division, Engineering Department, University of Cambridge, 9 J.J. Thomson Avenue, Cambridge CB3 0FA, UK*

[3] *Department of Electrical and Computer Engineering, Wilkes University, Wilkes-Barre, PA 18766, USA*

Correspondence should be addressed to Vijay K. Arora, vijay.arora@wilkes.edu

The carriers in a carbon nanotube (CNT), like in any quasi-1-dimensional (Q1D) nanostructure, have analog energy spectrum only in the quasifree direction; while the other two Cartesian directions are quantum-confined leading to a digital (quantized) energy spectrum. We report the salient features of the mobility and saturation velocity controlling the charge transport in a semiconducting single-walled CNT (SWCNT) channel. The ultimate drift velocity in SWCNT due to the high-electric-field streaming is based on the asymmetrical distribution function that converts randomness in zero-field to a stream-lined one in a very high electric field. Specifically, we show that a higher mobility in an SWCNT does not necessarily lead to a higher saturation velocity that is limited by the mean intrinsic velocity depending upon the band parameters. The intrinsic velocity is found to be appropriate thermal velocity in the nondegenerate regime, increasing with the temperature, but independent of carrier concentration. However, this intrinsic velocity is the Fermi velocity that is independent of temperature, but depends strongly on carrier concentration. The velocity that saturates in a high electric field can be lower than the intrinsic velocity due to onset of a quantum emission. In an SWCNT, the mobility may also become ballistic if the length of the channel is comparable or less than the mean free path.

1. INTRODUCTION

Due to the chemical stability and perfection of the carbon nanotube (CNT) structure, carrier mobility is not affected by processing and roughness scattering as it is in the conventional semiconducting channel. The fact that there are no dangling bond states at the surface of CNT allows for a wide choice of gate insulators in designing a field effect transistor (FET). It is not surprising that the CNTs are being explored as viable candidates for high-speed applications. The growing demand for higher computing power, smaller size, and lower power consumption of integrated circuits leads to a pressing need to downscale semiconductor components leading to novel new nanostructures [1]. CNTs, originally discovered by Iijima [2], have opened a number of applications. Some of these applications are building block of nano-VLSI circuit design, including reliable interconnects. The circuits so designed are shown to be mechanically rigid and able to carry high current densities. However, almost all synthetic methods result in bundles of CNTs rather than a well-organized strand requiring a complicated chemical procedure in separating individual single-walled CNT (SWCNT) that almost certainly would introduce damages of varying degrees. Peng et al. [3] have directly obtained soot from a chemical vapor deposition chamber. By fixing one end of the soot, a CNT (in their case a multiwall CNT) was drawn by using scanning electron microscope (SEM) nanoprobe. Electronic transport in these CNTs is in its infancy and needs to be investigated in order to develop novel application, for example, making a CNT FET. This is the motivation for this work.

The most nanoelectronic applications look for high-speed CNTs that are well known to have very high mobilities. The low scattering probability in CNTs is responsible for superior mobilities [4]. However, the work of Ahmadi et al. in a quantum nanowire (NW) has shown that the ultimate
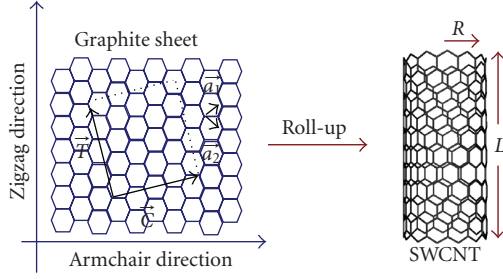
FIGURE 1: A prototype single-walled carbon nanotube with length $L \gg \lambda_D$, de Broglie wavelength, and $d = 2R \ll \lambda_D$.

saturation velocity does not sensitively depend on the low-field mobility. It is, therefore, of interest for us to find the ultimate velocity that may exist in an SWCNT. This velocity will necessarily depend on the band structure, the temperature, and the degeneracy level. The carrier drift is the velocity with which a carrier (electron or hole) can propagate through the length of the device encountering collisions on the way and starting its journey fresh on facing a collision. The higher mobility may bring an electron closer to saturation as a high electric field is encountered, but needs not to elevate the saturation velocity [5]. The reduction in conducting channel length of the device results in a reduced transit-time-delay and hence enhanced operational frequency. However, if the length is made smaller than the mean free path, the mobility may also become ballistic, free from randomizing scattering events.

In the following sections, the formalism is developed to study the velocity response to the electric field in an SWCNT as shown in Figure 1. The radius that is a few nanometers in size is comparable to de Broglie wavelength while length can vary from cm to μm range. This makes CNT a quasi-1-dimensional (Q1D) entity.

2. Q1D-CNT NANOSTRUCTURE

A single-walled carbon nanotube (SWCNT) of Figure 1 is a sheet of graphite (called graphene) rolled up into a cylinder with diameter of the order of a nanometer. For an electron on the surface of the CNT, it is certain to have wave properties as the diameter is comparable to de Broglie wavelength $\lambda_D = h/p$, where p is the carrier momentum. The tube diameter must necessarily contain integer (n) number of de Broglie waves for an electron to form a standing wave pattern around the rim of the CNT, thereby giving a resonant condition as the returning wave to the same point reinforces the electron motion. This constructive interference, leading to the resonant behavior, gives

$$2\pi R = n\frac{h}{p}, \quad n = 1, 2, 3 \ldots. \tag{1}$$

The quantized energy that depends on (1) relies on the relationship between energy and momentum that can be linear or quadratic depending on the chirality of the CNT. In order to understand the fundamentals of transport parameters without getting into the bandstructure complexities,

we will assume quadratic relationship as in a nanowire [6] for transverse energy. In this approximation, we consider transverse effective mass $m_{\perp}^{*}$ to be isotropic that depends on the diameter of the CNT [7] but independent of energy or momentum. The transverse energy of the CNT is given by

$$E_{\perp n} = \frac{n^2\hbar^2}{2m^*R^2}, \quad n = 1, 2, 3 \ldots. \tag{2}$$

In the longitudinal direction, the electron waves are propagating that result in the charge transport. With unaltered conduction band at E_{co}, the transverse energy in y and z directions is digital in nature as given by (2), but is of continuous analog-type in the longitudinal direction (taken to be x axis). The total energy is given by [8]

$$E = E_{co} + E_1 + \frac{\hbar^2 k_x^2}{2m^*} = E_c + \frac{\hbar^2 k_x^2}{2m^*}. \tag{3}$$

The chiral vector $\vec{C}$ specifies the direction of the roll-up:

$$\vec{C} = n\vec{a}_1 + m\vec{a}_2 = (n, m). \tag{4}$$

Here, $\vec{a}_1$ and $\vec{a}_2$ are the basis vectors of the lattice. In the (n, m) notation for $\vec{C}$, when $(n - m)$ is a multiple of 3 the nanotube is metallic, the vectors $(n, 0)$ or $(0, m)$ denote zigzag CNTs, whereas the vectors (n, m) correspond to chiral CNTs. In the semiconducting mode of CNT, as in $(5, 3)$ chirality, the band structure can be manipulated to be parabolic in the semiconducting mode of operation. Due to the approximation for the graphene band structure near the Fermi point, the $E(k)$ relation of the CNT is

$$E(\vec{k}) = t\frac{3a_{C-C}}{2}|\vec{k}_{CN}| = \frac{t3a_{C-C}}{2}\sqrt{k_{cv}^2 + k_t^2}, \tag{5}$$

where k_{cv} is the wave vector component along the circular direction, which is quantized by the periodic boundary condition, and k_t is the wave vector along the length of the CNT. Also, k_{cv} is minimum for the lowest band of CNT. The minimum value for k_{cv} is zero for the metallic CNT. Therefore, the density of states (DOS) is given by

$$D(E) = D_0 = \frac{8}{3a_{C-C}t\pi}, \tag{6}$$

where $a_{C-C} = 1.42$ Å is the carbon-carbon (C–C) bond length, $t = 2.7$ eV [9, 10] is the nearest neighbor C–C tight binding overlap energy, and d is the diameter of the carbon nanotube, taken to be that of $(5, 3)$ chirality.

The band structure is indeed nonparabolic. However, for low-lying states in the vicinity of $k = 0$, where most electrons reside, the band structure is approximately parabolic, as shown in Figure 2. For the semiconducting CNT, the focus of our study, the minimum magnitude of the circumferential wave vector is $k_{cv} = 2/3d$, where $d = 2R$ is the diameter of the CNT. By substituting this equation into the $E(k)$ approximation for the semiconducting CNT, we get

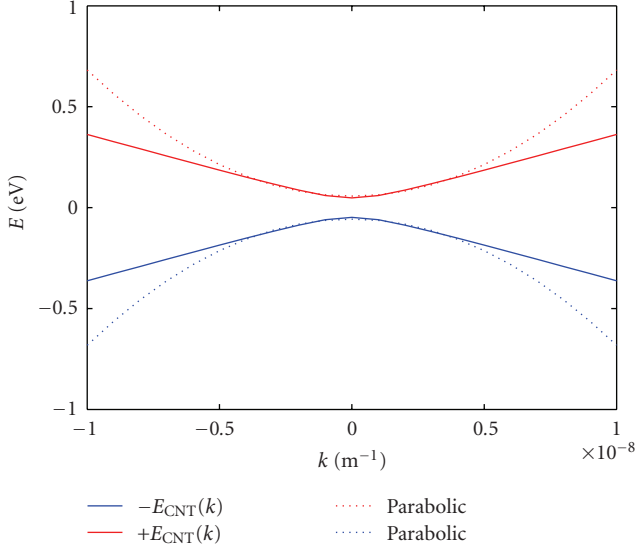$$E(k) = \pm\frac{t3a_{C-C}}{2}\sqrt{\left(\frac{2}{3d}\right)^2 + k_t^2}. \tag{7}$$

FIGURE 2: The parabolic band structure of CNT in the vicinity of energy minimum ($k = 0$) with conduction and valence bands separated by the first bandgap E_G.
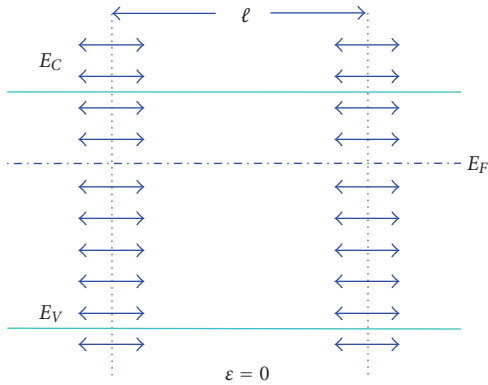

FIGURE 3: The flat-band diagram for CNT in equilibrium.

Near the band minimum, all metallic and semiconducting annotates are equivalent. According to (5), the conduction and valence bands of a semiconducting CNT are mirror image of each other and the first band gap is $E_G = 2a_{C-C}t/d = 0.8(ev)/d(nm)$.

In this description, the energy $E(k)$ and band gap in semiconducting CNT are function of diameter. There are higher-order subbands that may be populated as well. However, (5) when $k_x d \ll 1$ reduces to

$$E(k) = \frac{E_G}{2}\sqrt{1 + \left(\frac{3k_x d}{2}\right)^2} \approx \frac{E_G}{2}\left(1 + \frac{9}{8}d^2 k_x^2\right), \quad (8)$$

where E_G is the CNT bandgap and d is the diameter. When expanded to the first order, the E-k relation becomes as in (3) with $E_{co} = E_G/2$. With this modification, m^* in (3) is the

longitudinal effective mass that depends on the diameter of the tube:

$$\frac{m^*}{m_0} = \frac{4\hbar^2}{9a_{C-C}dt} = \frac{0.08 \text{ nm}}{d \text{ (nm)}}. \quad (9)$$

In one-dimensional carbon nanotube using (5) for the gradient of k, definition of density of states DOS, including effect of the electron spin, leads to the following equation which is similar to that in Q1D nanowire [11]:

$$\text{DOS} = \frac{\Delta n_x}{\Delta E L_x} = \frac{1}{2\pi}\left(E - \frac{E_G}{2}\right)^{-1/2}\left(\frac{2m^*}{\hbar^2}\right)^{1/2}. \quad (10)$$

As in any Q1D, DOS diverges at the bandedge $E = E_c$ but drops as square root of the kinetic energy $E_k = E - E_c$.

3. ENERGY AND VELOCITY DISTRIBUTION

The distribution function of the energy E_k is given by the Fermi-Dirac distribution function:

$$f(E_k) = \frac{1}{e^{(E_k - E_{F1})/k_B T} + 1}, \quad (11)$$

where E_{F1} is the Fermi energy that is equivalent to chemical potential and describes the degeneracy nature of the electron concentration. As shown in Figure 3, the Fermi energy level runs parallel to the conduction band edge. The Fermi level is in the bandgap for the nondegenerate carrier concentration and within the conduction (or valence) band for degenerate carrier (electron or hole) concentration. In the absence of electric field, the bands are flat. The velocity vectors for the randomly moving stochastic electrons cancel each other giving net drift equal to zero, as shown in the flat band diagram of Figure 3. In a homogenous CNT, equal numbers from left and right are entering the free path.

This random motion does not mean that the magnitude of a single vector (that we call the intrinsic velocity) is zero. The average of this intrinsic velocity v_{i1}, as calculated from the average value of $|v|$ with the distribution function of (11) multiplied by the DOS of (10), is given by

$$v_{i1} = v_{th1}\frac{\Im_o(\eta_1)}{\Im_{-1/2}(\eta_1)} \quad (12)$$

with

$$\Im_j(\eta) = \frac{1}{\Gamma(j+1)}\int_0^\infty \frac{x^j}{e^{(x-\eta)} + 1}dx, \quad (13)$$

$$v_{th1} = \frac{1}{\sqrt{\pi}}v_{th} = \frac{1}{\sqrt{\pi}}\sqrt{\frac{2k_B T}{m^*}}. \quad (14)$$

The normalized Fermi energy $\eta_1 = (E_{F1} - E_c)/k_B T$ is calculated from the carrier concentration n_1 per unit length of the CNT as follows:

$$n_1 = N_{c1}\Im_{-1/2}(\eta_1) \quad (15)$$

with

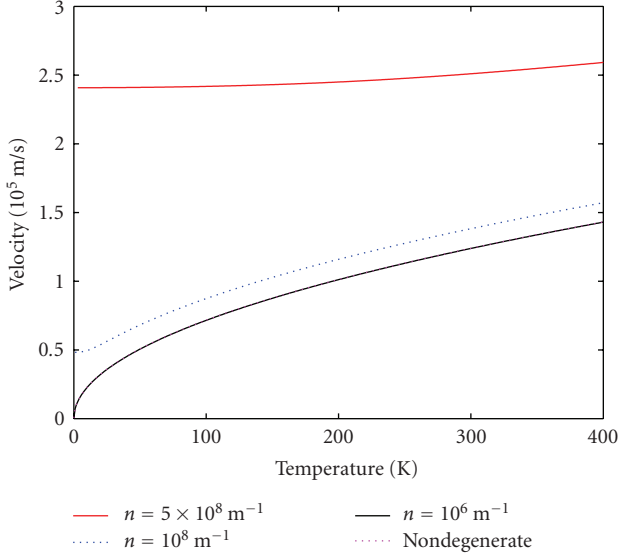$$N_{c1} = \left(\frac{2m^* k_B T}{\pi\hbar^2}\right)^{1/2}. \quad (16)$$

FIGURE 4: Intrinsic velocity versus temperature for $(5, 3)$ CNT for three concentration values. Also shown is the nondegenerate limit.

FIGURE 5: Velocity versus carrier concentration for $T = 4.2\,K$ (liquid helium), $T = 77\,K$ (liquid nitrogen), and $T = 300\,K$ (room temperature). The 4.2 K curve is closer to the degenerate limit.

Here, $\Im_j(\eta)$ is the Fermi-Dirac integral of order j and $\Gamma(j+1)$ is a Gamma function of order $j + 1$. Its value for an integer j is $\Gamma(j + 1) = j\Gamma(j) = j!$. The value of Γ for $j = 0$ is $\Gamma(1) = 1$ and for $j = -1/2$ is $\Gamma(1/2) = \sqrt{\pi}$. The Fermi integral with Maxwellian approximation is always an exponential for all values of j and is given by [12]

$$\Im_j(\eta) = e^\eta \quad \text{(nondegenerate)}. \tag{17}$$

In the strongly degenerate regime, the Fermi integral transforms to

$$\Im_j(\eta) = \frac{1}{\Gamma(j + 1)} \frac{\eta^{j+1}}{j + 1} = \frac{\eta^{j+1}}{\Gamma(j + 2)} \quad \text{(deg)}. \tag{18}$$

The degeneracy of the carriers sets in at $n_1 = N_{c1} = 2.0 \times 10^8\,\text{m}^{-1}$ for Q1D-CNT with chirality $(5, 3)$ $(m^* = 0.189\,m_o)$ [13]. The carriers are nondegenerate if the concentration n_1 is less than this value and degenerate if it is larger than this value. The threshold for the onset of degeneracy will change as chirality changes. The effective mass is $m^* = 0.099\,m_o$ [13] for $(9, 2)$ chirality, and degeneracy sets in at $n_1 = 1.46 \times 10^8\,\text{m}^{-1}$.

Figure 4 indicates the ultimate velocity as a function of temperature. Also shown is the graph for nondegenerate approximation. The velocity for low carrier concentration follows $T^{1/2}$ behavior independent of carrier concentration. As concentration is increased to embrace degenerate domain, the intrinsic velocity tends to be independent of temperature, but depends strongly on carrier concentration. The nondegenerate limit of intrinsic velocity v_{i1} is $v_{\text{th}1}$ of (14). Figure 5 shows the graph of ultimate intrinsic velocity as a function of carrier concentration for three temperatures $T = 4.2\,K$ (liquid helium), 77 K (liquid nitrogen), and 300 K (room temperature). As expected, at low temperature, carriers follow the degenerate statistics and hence their velocity is
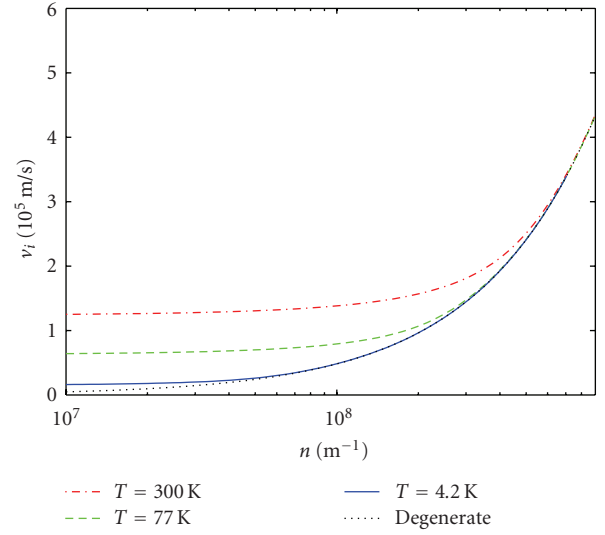
limited by appropriate average of the Fermi velocity that is a function of carrier concentration. In the degenerate limit, the intrinsic velocity is only the function of carrier concentration and is independent of temperature:

$$v_{i1\text{Deg}} = \frac{\hbar}{4m^*}(n_1\pi). \tag{19}$$

Equation (19) shows that the intrinsic velocity is a linear function of the linear carrier concentration, as shown in Figure 5. However, it may be affected by the onset of a quantum emission. For low carrier concentrations, the velocity is independent of carrier concentration as the graphs are flat. Most published works tend to use thermal velocity for modeling as it is independent of carrier concentration.

4. HIGH-FIELD DISTRIBUTION

Arora [14] modified the equilibrium distribution function of (11) by replacing E_{F1} (the chemical potential) with the electrochemical potential $E_{F1} + q\,\vec{\varepsilon}\cdot\vec{\ell}$. Here, $\vec{\varepsilon}$ is the applied electric field, q is the electronic charge, and $\vec{\ell}$ the mean free path during which carriers are collision free or ballistic. Arora's distribution function is thus given by

$$f(E_k) = \frac{1}{e^{(E_k - E_{F1} + q\vec{\varepsilon}\cdot\vec{\ell})/k_B T} + 1}. \tag{20}$$

This distribution has simpler interpretation as given in the tilted-band diagram of Figure 6. A channel of CNT can be thought as a series of ballistic resistors each of length ℓ, where the ends of each free path can be considered as virtual contacts with different quasi-Fermi levels separated in energy by $q\,\vec{\varepsilon}\cdot\vec{\ell}$. It is clear that this behavior is compatible with the transport regime in a single ballistic channel where
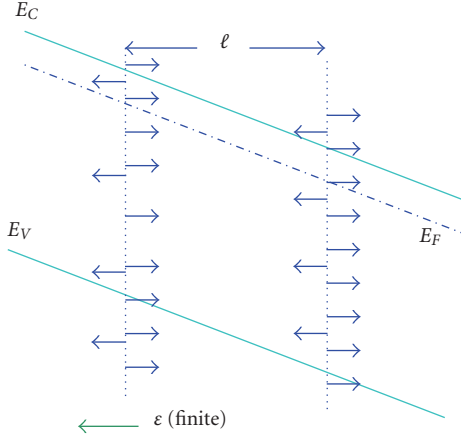
FIGURE 6: Partial stream-lining of electron motion on a tilted band diagram in an electric field.

FIGURE 7: Conversion of random velocity vectors to the stream-lined one in an infinite electric field.

local quasi-Fermi level can be defined on both ends for the source and drain contacts. This behavior is understandable if we consider the widely diffused interpretation of inelastic scattering represented by the Büttiker approach of virtual thermalizing probes [15], which can be used to describe transport in any regime. Within this approach, carriers are injected into a "virtual" reservoir where they are thermalized and start their ballistic journey for the next free path. The carriers starting from the left at Fermi potential E_{F1} end the free-path voyage with $E_{F1} - q\, \vec{\varepsilon}\vec{\ell}$. Those starting from right end of the free path end the voyage with the electrochemical potential $E_{F1} + q\, \vec{\varepsilon}\vec{\ell}$. These are the two quasi-Fermi levels. The current flow is due to the gradient of the Fermi energy $E_{F1}\,(x)$ in the presence of an electric field. Because of this asymmetry in the distribution of electrons, the electrons in Figure 6 tend to drift opposite to the electric field $\vec{\varepsilon}$ applied in the negative x-direction (right to left).

In an extremely large electric field, virtually all the electrons are traveling in the positive x-direction (opposite to the electric field), as shown in Figure 7. This is what is meant by conversion of otherwise completely random motion into a stream-lined one with ultimate velocity per electron equal to v_i. Hence, the ultimate velocity is ballistic independent of scattering interactions. This interpretation is consistent with the laws of quantum mechanic where the propagating electron waves in the direction of the electric field find it hard to surmount the infinite potential barrier and hence are reflected back elastically with the same velocity.

The ballistic motion in a free path may be interrupted by the onset of a quantum emission of energy $\hbar\omega_o$. This quantum may be an optical phonon or a photon or any digital energy difference between the quantized energy levels with or without external stimulation present. The mean-free path with the emission of a quantum of energy is related to ℓ_0 (zero-field mean free path) by an expression [16]

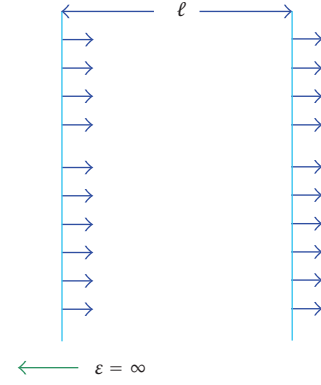$$\ell = \ell_0\left[1 - e^{-E_Q/q\varepsilon\ell_0}\right] = \ell_0\left[1 - e^{-\ell_Q/\ell_0}\right] \qquad (21)$$

with

$$q\varepsilon\ell_Q = E_Q = (N_0 + 1)\hbar\omega_0,$$
$$N_0 = \frac{1}{e^{\hbar\omega_0/k_BT} - 1}. \qquad (22)$$

Here, $(N_o + 1)$ gives the probability of a quantum emission. N_o is the Bose-Einstein distribution function determining the probability of quantum emission. The degraded mean free path ℓ is now smaller than the low-field mean free path ℓ_o. Also, $\ell \approx \ell_o$ in the ohmic low-field regime as expected. In high electric field, $\ell \approx \ell_Q$. The inelastic scattering length during which a quantum is emitted is given by

$$\ell_Q = \frac{E_Q}{q\varepsilon}. \qquad (23)$$

Obviously, $\ell_Q = \infty$ in zero electric field and will not modify the traditional scattering described by mean free path ℓ_0 as $\ell_Q \gg \ell_0$. The low-field mobility and associated drift motion are, therefore, scattering-limited. The effect of all possible scattering interactions in the ohmic limit is buried in the mean free path ℓ_0. The nature of the quantum emitted depends on the experimental set up and the presence of external stimulations as well as the spacing between the digitized energies. This quantum may be in the form of a phonon, photon, or the spacing with the quantized energy of the two lowest levels. For the quantum emission to be initiated by transition to higher quantum state with subsequent emission to the lower state, the quantum energy $\hbar\omega_o = \Delta E_{\perp 1-2}$ is a function of radius of the CNT:

$$\hbar\omega_o = \frac{3\hbar^2}{2m^*R^2}. \qquad (24)$$

This dependence of the quantum on the radius or diameter of the CNT may give an important clue about the CNT chirality and could be used for characterization of the CNT.

The number of electrons in each direction is proportional to $e^{\pm q\varepsilon\ell/k_BT}$ (+ sign is for antiparallel and − sign is for parallel
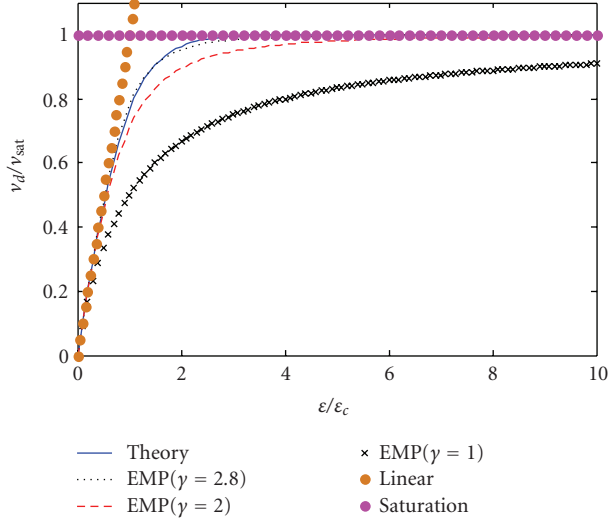
FIGURE 8: Normalized velocity-field characteristics for an SWCNT as predicted from the theory and compared with empirical models.

direction). The number of antiparallel electrons overwhelms due to rising exponential and those in parallel direction decrease to virtually zero due to the decaying exponential. The net fraction F_{ant} of the stream-lined electrons is then given by

$$F_{ant} = \frac{e^{q\varepsilon\ell/k_B T} - e^{-q\varepsilon\ell/k_B T}}{e^{q\varepsilon\ell/k_B T} + e^{-q\varepsilon\ell/k_B T}} = \tanh\left(\frac{q\varepsilon\ell}{k_B T}\right). \qquad (25)$$

When the net velocity response to the electric filed for the fraction of electrons drifting in the opposite (antiparallel) direction of the electric field is considered, the drift response is obtained as [17]

$$v_d = v_{sat} \tanh\left(\frac{q\mathcal{E}\ell}{k_B T}\right) = v_{sat} \tanh\left(\frac{\mathcal{E}}{\mathcal{E}_c}\right) \qquad (26)$$

with

$$\mathcal{E}_c = \frac{k_B T}{q\ell} = \frac{V_t}{\ell}, \qquad (27)$$

where $\mathcal{E}_c$ is the critical electric field for the onset of nonohmic behavior. Also, $V_t = k_B T/q$ is the thermal voltage whose value at the room temperature is 0.0259 V.

Figure 8 gives the normalized plot of v_d/v_{sat} versus $\varepsilon/\varepsilon_c$. Also, $v_{sat} = v_{i1}$ when quantum emitted has energy much higher than the thermal energy ($\hbar\omega_o \gg k_B T$). The saturation velocity $v_{sat} = v_{i1} \tanh(\hbar\omega_o/k_B T)$ when $\hbar\omega_o$ is comparable to the thermal energy $k_B T$. Figure 8 shows the comparison with the empirical equation normally employed in the simulation programs:

$$v_d = v_{sat} \frac{1}{\left[1 + (\mathcal{E}/\mathcal{E}_c)^\gamma\right]^{1/\gamma}}, \qquad (28)$$

where γ is a parameter. A wide variety of parameters are quoted in the published literature. Greenberg and del Alamo

[18] give convincing evidence from measurements on a 5 μm InGaAs resistive channel that $\gamma = 2.8$. Other values that are commonly quoted are $\gamma = 2$ for electrons and $\gamma = 1$ for holes. The discrepancy arises from the fact that it is impossible to measure directly the saturation velocity that requires an infinite electric field. No device is able to sustain such a high electric field. The ultimate saturation velocity then can be obtained only indirectly. Normally, the highest measured drift velocity is ascribed to be the saturation velocity which is always lower than the actual saturation velocity. The plots differ only at the intermediate values of the electric field.

In the low-field limit, velocity-field graph is linear from which ohmic mobility can be obtained. Chai et al. [19] have demonstrated transport of energetic electrons through aligned tubes with lengths of 0.7–3 mm. These developments open the possibility of ballistic mobility as suggested by Wang and Lundstrom [20] and Shur [21]. In fact, Mugnaini and Iannaccone [22, 23] have done a study of transport ranging from drift-diffusion to ballistic. Their model is also applicable to nanowires and CNTs which is similar to the Büttiker approach to dissipative transport [15]. In principle, our formalism is very similar to that of Mugnaini and Iannaccone. In all these works, analytical results obtained for nano-MOSFET are consistent with that for ballistic nanowire transistors [5, 6] and also for the CNT nanostructures reported here. In this scenario, generic resistive channel of a CNT can be described as a series of resistive channels each with a finite scattering length ℓ. Since L can be as low as 0.7 μm that can be lower than the mean free path in a CNT because of extremely high mobility, it is worthwhile to evaluate how the mobility will change in a ballistic channel with $L < \ell$. This relation between the mobility, the mean free path ℓ, and the channel length L is expected to have deeper consequences on the understanding of transport in nanostructured devices.

The long-channel mobility μ_∞ as obtained from low-field approximation of (26) is given by

$$\mu_\infty = \frac{q\ell}{m^* v_m}, \quad v_m = \frac{v_{th}^2}{2v_{sat}}, \qquad (29)$$

where v_m is the mobility velocity that is a combination of thermal hop on thermalization and v_{sat} that arises in the middle of the free path. In a short-channel CNT, even the mobility may become ballistic. The length-limited ballistic mobility μ_L can be obtained similar to the technique used for the scattering length for the emission [11] of a quantum and is obtained as

$$\mu_L = \mu_\infty (1 - e^{-L/\ell}). \qquad (30)$$

In the limit that the length L of the CNT is smaller than the mean free path, the mobility will also become ballistic replacing mean free path ℓ in (30) with L. This gives ballistic mobility:

$$\mu_B = \frac{qL}{m^* v_m}. \qquad (31)$$

Now the mobility is limited by only the length of the channel and ballistic intrinsic velocity that is a function of temperature and carrier concentration.
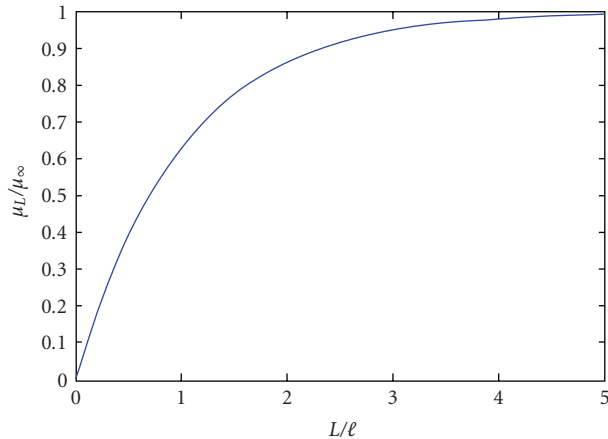
FIGURE 9: Normalized length-limited mobility to that in an infinite sample versus normalized length of the CNT to that of the mean free path in the CNT.

Figure 9 gives the normalized plot of μ_L/μ_∞ versus L/ℓ. It is clear from the graph that the relative mobility approaches unity in the long-channel limit $L \gg \ell$. However, in the short channel limit ($L \ll \ell$), the relative mobility is a linear function of length of the CNT.

5. CONCLUSION

As the scaling of devices continues and new nanostructures like CNT are discovered and exploited for experimentation, more challenges as well as opportunities appear to extend the vision encountered in the International Technology Roadmap for Semiconductors [24]. CNT devices have attracted a lot of attention because of their ideal electronic properties. Both p- and n-type CNT-FET have been fabricated and have exhibited promising characteristics. However, the device physics and transport mechanisms of such devices are not yet fully understood. The results presented here will enhance the efforts that have been put on modeling CNT-FETs. Nonequilibrium Green's function approach [7] is too cumbersome to understand the physical processes controlling the transport in Q1D nanostructure. The developed paradigm provides simple intuitive description of the Q1D device physics that is easily implementable.

Starting from a model for ballistic one-dimensional FET model and adopting the Büttiker probes interpretation of inelastic scattering, we have shown that the case of intermediate transport between fully ballistic transport and drift-diffusion transport can be described by the series of an equivalent drift-diffusion minichannels with a ballistic transport, consistently with the earlier results obtained in the ohmic domain [25–28]. Therefore, this compact macromodel can be considered an adequate description of transport in nanoscaled CNT. In fact, our model embraces virtually all nanostructures. In the presence of a magnetic field [26], the spiraled path of a carrier will have similar transport mechanism as pointed out here.

The asymmetrical distribution function reported here is a very valuable tool for studying quantum transport in nanostructures. This distribution function takes into account the asymmetrical distribution of drifting electrons or holes in an electric field. This distribution function transforms the random motion of electrons into a stream-lined one that gives the ultimate saturation velocity that is a function of temperature in nondegenerate regime and a function of carrier concentration in the degenerate regime. The ultimate drift velocity is found to be appropriate thermal velocity for nondegenerately doped CNTs. However, the ultimate drift velocity is the Fermi velocity for degenerately-doped Q1D CNTs. The inclusion of quantum emission for a given sample may further highlight the fundamental physical processes that are present. We also show the insensitivity of the saturation velocity on ohmic mobility that is scattering-limited. Even for the ohmic mobility, we have extended the vision to embrace ballistic mobility that will be independent of scattering when the channel length is smaller than the scattering-dependent mean free path.

It is our hope that these results will be liberally utilized for modeling, simulations, characterization, and extraction of device parameters without ambiguity.

REFERENCES

[1] M. Pourfath, H. Kosina, and S. Selberherr, "Numerical study of quantum transport in carbon nanotube transistors," *Mathematics and Computers in Simulation*. In press.

[2] S. Iijima, "Helical microtubules of graphitic carbon," *Nature*, vol. 354, no. 6348, pp. 56–58, 1991.

[3] L.-M. Peng, Q. Chen, X. L. Liang, et al., "Performing probe experiments in the SEM," *Micron*, vol. 35, no. 6, pp. 495–502, 2004.

[4] R. Martel, T. Schmidt, H. R. Shea, T. Hertel, and Ph. Avouris, "Single- and multi-wall carbon nanotube field-effect transistors," *Applied Physics Letters*, vol. 73, no. 17, pp. 2447–2449, 1998.

[5] M. T. Ahmadi, H. H. Lau, R. Ismail, and V. K. Arora, "Current-voltage characteristics of a silicon nanowire transistor," *Microelectronics Journal*. In press.

[6] M. T. Ahmadi, M. L. P. Tan, R. Ismail, and V. K. Arora, "The high-field drift velocity in degenerately-doped silicon nanowires," to appear in *International Journal of Nanotechnology*.

[7] M. S. Lundstrom and J. Guo, *Nanoscale Transistors: Device Physics, Modeling and Simulation*, Springer, New York, NY, USA, 2006.

[8] M. Lundstrom, "Elementary scattering theory of the Si MOSFET," *IEEE Electron Device Letters*, vol. 18, no. 7, pp. 361–363, 1997.

[9] R. A. Jishi, D. Inomata, K. Nakao, M. S. Dresselhaus, and G. Dresselhaus, "Electronic and lattice properties of carbon nanotubes," *Journal of the Physical Society of Japan*, vol. 63, no. 6, pp. 2252–2260, 1994.

[10] J. W. G. Wildöer, L. C. Venema, A. G. Rinzler, R. E. Smalley, and C. Dekker, "Electronic structure of atomically resolved carbon nanotubes," *Nature*, vol. 391, no. 6662, pp. 59–62, 1998.

[11] V. K. Arora, "Quantum engineering of nanoelectronic devices: the role of quantum emission in limiting drift velocity and diffusion coefficient," *Microelectronics Journal*, vol. 31, no. 11-12, pp. 853–859, 2000.

[12] V. K. Arora, "High-field distribution and mobility in semiconductors," *Japanese Journal of Applied Physics*, vol. 24, no. 5, pp. 537–545, 1985.

[13] J. M. Marulanda and A. Srivastava, "Carrier density and effective mass calculations for carbon nanotubes," in *Proceedings of IEEE International Conference on Integrated Circuit Design and Technology (ICICDT 07)*, pp. 234–237, Austin, Tex, USA, May 2007.

[14] V. K. Arora, "Failure of Ohm's law: its implications on the design of nanoelectronic devices and circuits," in *Proceedings of the 25th International Conference on Microelectronics (MIEL 06)*, pp. 15–22, Nis, Serbia, May 2006.

[15] M. Büttiker, "Role of quantum coherence in series resistors," *Physical Review B*, vol. 33, no. 5, pp. 3020–3026, 1986.

[16] V. K. Arora, "Drift diffusion and Einstein relation for electrons in silicon subjected to a high electric field," *Applied Physics Letters*, vol. 80, no. 20, pp. 3763–3765, 2002.

[17] V. K. Arora, M. L. P. Tan, I. Saad, and R. Ismail, "Ballistic quantum transport in a nanoscale metal-oxide-semiconductor field effect transistor," *Applied Physics Letters*, vol. 91, no. 10, Article ID 103510, 3 pages, 2007.

[18] D. R. Greenberg and J. A. del Alamo, "Velocity saturation in the extrinsic device: a fundamental limit in HFET's," *IEEE Transactions on Electron Devices*, vol. 41, no. 8, pp. 1334–1339, 1994.

[19] G. Chai, H. Heinrich, L. Chow, and T. Schenkel, "Electron transport through single carbon nanotubes," *Applied Physics Letters*, vol. 91, no. 10, Article ID 103101, 3 pages, 2007.

[20] J. Wang and M. Lundstrom, "Ballistic transport in high electron mobility transistors," *IEEE Transactions on Electron Devices*, vol. 50, no. 7, pp. 1604–1609, 2003.

[21] M. S. Shur, "Low ballistic mobility in submicron HEMTs," *IEEE Electron Device Letters*, vol. 23, no. 9, pp. 511–513, 2002.

[22] G. Mugnaini and G. Iannaccone, "Physics-based compact model of nanoscale MOSFETs—part I: transition from drift-diffusion to ballistic transport," *IEEE Transactions on Electron Devices*, vol. 52, no. 8, pp. 1795–1801, 2005.

[23] G. Mugnaini and G. Iannaccone, "Physics-based compact model of nanoscale MOSFETs—part II: effects of degeneracy on transport," *IEEE Transactions on Electron Devices*, vol. 52, no. 8, pp. 1802–1806, 2005.

[24] A. Hazeghi, T. Krishnamohan, and H.-S. P. Wong, "Schottky-barrier carbon nanotube field-effect transistor modeling," *IEEE Transactions on Electron Devices*, vol. 54, no. 3, pp. 439–445, 2007.

[25] V. K. Arora and M. Prasad, "Quantum transport in quasi-one-dimensional systems," *Physica Status Solidi B*, vol. 117, no. 1, pp. 127–140, 1983.

[26] V. K. Arora, "Quantum and classical-limit longitudinal magnetoresistance for anisotropic energy surfaces," *Physical Review B*, vol. 26, no. 12, pp. 7046–7048, 1982.

[27] V. K. Arora, "Quantum size effect in thin-wire transport," *Physical Review B*, vol. 23, no. 10, pp. 5611–5612, 1981.

[28] V. K. Arora, "Quantum well wires: electrical and optical properties," *Journal of Physics C*, vol. 18, no. 15, pp. 3011–3016, 1985.